Available online at www.eccomasproceedia.org
Eccomas Proceedia COMPDYN (2023) 1016-1030

ECCOMAS
Proceedia

COMPDYN 2023
9th ECCOMAS Thematic Conference on
Computational Methods in Structural Dynamics and Earthquake Engineering
M. Papadrakakis, M. Fragiadakis (eds.)
Athens, Greece, 12-14 June 2023

ON THE VIBRATION ATTENUATION PERFORMANCE OF A GEOMETRICALLY NONLINEAR DEVICE MOUNTED TO A MULTI-STOREY STRUCTURE

Kyriakos Alexandros Chondrogiannis[1], **Vasilis Dertimanis**[1], **and Eleni Chatzi**[1]

[1]Department of Civil, Environmental and Geomatic Engineering, ETH Zürich
Stefano-Franscini-Platz 5, 8093 Zurich, Switzerland
e-mail: {Chondrogiannis, v.derti, chatzi}@ibk.baug.ethz.ch

Abstract. *Structures should adhere to capacity and serviceability requirements that can be compromised by dynamic excitation. Structural vibration mitigation aims to ensure serviceability and guarantee safety, but often suffers from limitations of the enabling devices; usually preferred to follow a passive scheme. The current study harnesses the potential of nonlinear mechanisms to amplify the vibration mitigation effects. A geometrically nonlinear device is proposed, called NegSV, which is mounted on a frame structure, without requirement of an additional tunable mass mechanism. The nonlinear configuration leads to negative stiffness phenomena, which can be exploited for guiding the input energy toward specific structural elements. The dynamics of the system and its efficacy in terms of vibration attenuation is studied via nonlinear finite element analyses under base excitation. The seismic input is additionally parametrized in order to allow for a probabilistic assessment of its influence on the performance of the device, via use of Monte Carlo simulations. The probabilistic distributions of associated structural integrity metrics are calculated on the basis of assumed distributions of the input parameters. The respective results for both the unprotected and protected structures are compared, revealing effective vibration mitigation potential for critical system components, such as the base of the structure, relieving base shear.*

Keywords: Negative stiffness, Geometric nonlinearities, Vibration mitigation, Structural protection

ISSN:2623-3347
Peer-review under responsibility of the organizing committee of COMPDYN 2023.
doi: 10.7712/120123.10454.20652

1 INTRODUCTION

Structural safety, within the seismic context, can be effectuated via appropriate vibration control and mitigation mechanisms [1, 2, 3]. The design of such devices is subjected to particular requirements with respect to the frequency content of the seismic input, which usually lies at the lower range, as well as to the aspect of dealing with protected systems of large mass [4]. Due to reasons related to their cost, low energy requirements and low complexity, passive vibration devices are often preferred. These are typically distinguished in two major categories; energy transfer mechanisms to a secondary attachment, or base isolation techniques. An established solution of the targeted energy transfer strategy is the tuned mass damper [5]. According to this method, a linear oscillator is attached to a primary system and the natural frequency of the former is tuned to match the natural frequency of the latter. Energy transfer takes place at the resonance frequency, allowing for vibration mitigation. Base isolation methods rely on placement of bearings at the foundation level of the structure [6]. This has the effect of shifting the natural period of the combined system to a higher range, where the expected response is limited, as prescribed by response spectra according to provisions.

Whilst commonly preferred, passive vibration can come with limited attenuation potential. Recent works have demonstrated that exploitation of nonlinearity and negative stiffness can amplify the efficacy of passive vibration attenuation solutions [7]. Nonlinear targeted energy transfer [8] has been studied in the literature demonstrating potential toward improving the performance of passive energy absorbing devices. Al-Shudeifat [9] and Chen et al. [10] have studied the properties of a nonlinear energy sink, formed by a triangular arch arrangement, able to create a negative stiffness effect, where the ”restoring” force points to the same direction as the external loading, demonstrating its vibration mitigation capabilities. Nonlinearity and negative stiffness have also been studied in metamaterial configurations [11, 12, 13, 14], demonstrating potential towards structural applications of [15, 16] within the metabarrier and metafoundation context. Within the context of geometrically nonlinear mechanisms targeting a negative stiffness effect, the K-Damper device has been recently proposed [17, 18, 19]. This incorporates a negative stiffness element, which increases the channelling of energy to a secondary attachment.

In this work, we propose a vibration mitigation device, named NegSV, which introduces negative stiffness elements at the top storey of existing or new building structures, thus shifting the primary natural frequency to a lower range. Similarly to the partial mass isolation strategy [20, 21], the aim is to direct the input energy away from critical parts of the structure and achieve dissipation at specified locations. This brings in a requirement for increased displacement capacity at the modified storey which, although disadvantageous, is shown to comprise an effect that can be controlled to a certain extent. The performance of the system is evaluated via use of finite element analyses and lumped mass models under base excitation. In order to offer a generalized framework for quantifying the effects of the input onto the resulting performance, a stochastic input is considered, in terms of the seismic signal properties, and the reduction in the probability of failure is determined for the modified building system. It is observed that the nonlinear device can offer considerable vibration mitigation potential, thus reducing the relevant failure probability, based on the resulting inter-storey drifts. An important aspect is the ease of application of the system for retrofitting purposes, as it can be conveniently fitted to an existing building with moderate interference in terms of the serviceability of the modified floor.

2 NEGATIVE STIFFNESS DEVICE

2.1 Geometrically nonlinear element

The proposed geometrically nonlinear mechanism results from a triangular arch assembly, shown in Fig. 1, where two identical springs of constant k_d and natural length L_d are placed in a isosceles triangle arrangement of base $2L$ and height H. The equilibrium path of the element can be graphed according to Eq. (1), that provides an exact solution [11]. It can be observed that there exist two stable equilibrium positions for $\delta = 0$ and $\delta = 2H$ and one unstable equilibrium position for $\delta = H$. Interestingly, around the unstable position, negative stiffness is present, in the range where the slope of the equilibrium path takes negative values.

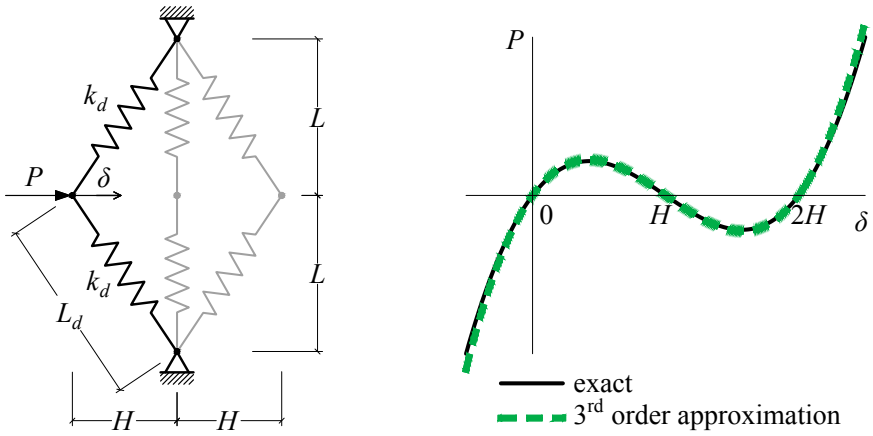

Figure 1: Geometrically nonlinear element. (left)-geometry, (right)-equilibrium path.

$$P = 2k_dL_d\left(1 - \sqrt{\frac{\left(\frac{L}{H}\right)^2 + \left(1 - \frac{\delta}{H}\right)^2}{\left(\frac{L}{H}\right)^2 + 1}}\right) \cdot \frac{1 - \frac{\delta}{H}}{\sqrt{\left(\frac{L}{H}\right)^2 + \left(1 - \frac{\delta}{H}\right)^2}}, \tag{1}$$

where $L_d = \sqrt{L^2 + H^2}$.

The nonlinear force-displacement relation can further be approximated via a 3rd order polynomial [9], performing Taylor series expansion around $\delta = H$, as follows:

$$\begin{aligned} P &\approx k_1(\delta - H) + k_2(\delta - H)^3, \\ k_1 &= -2k_d\left(\frac{L_d}{L} - 1\right), \\ k_2 &= \frac{k_dL_d}{L^3}. \end{aligned} \tag{2}$$

The slope of the equilibrium path at the unstable equilibrium position, for $\delta = H$, takes the negative value k_1, which will be used for proper tuning of the constructed device in the following sections.

2.2 Stiffness modification of an oscillator

The element described in Sec. 2.1 is exploited for the adjustment of an oscillator's stiffness. The nonlinear element is connected in parallel to the linear spring of an oscillator, as shown in Fig. 2a. The total restoring force F_{tot} is calculated as the sum of the linear force F_l and the nonlinear term F_{nl} and the corresponding equilibrium paths are given in Fig.2b. The linear curve F_l results from the linear spring of stiffness k, while the nonlinear curve F_{nl} corresponds to the equilibrium path of the triangular arch that has an initial displacement H and a negative stiffness value $k_1 = k_N$. Notice that the assembly of Fig. 2 is stable at $x = 0$ as long as the total stiffness of the system is positive for this position and for this purpose, it should hold that $k > |k_N|$. At this position, the tangential stiffness takes the value $k + k_N$, $k_N < 0$.

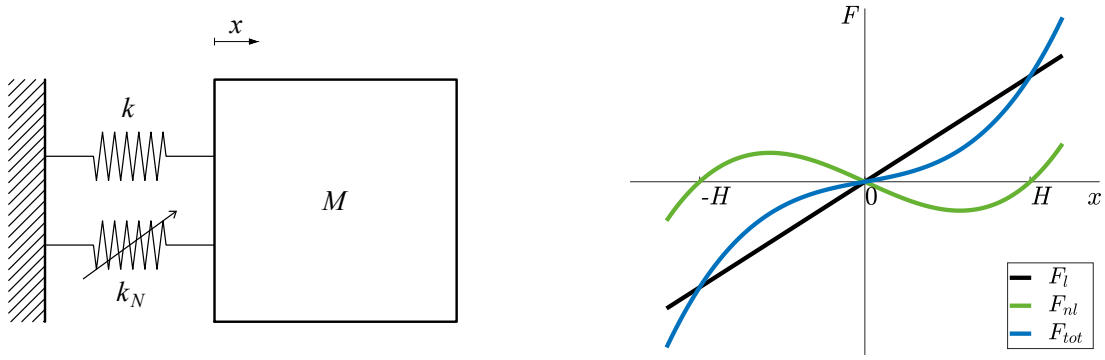

(a) Modified oscillator.

(b) Equilibrium path.

Figure 2: Schematic representation of stiffness adjustment via a negative stiffness element.

The modification of the stiffness of an oscillator can be used for adjusting its natural frequency, alleviating the need for mass alteration. Focusing on the single degree of freedom (sdof) system of Fig. 2a, the natural frequency of the linear oscillator, without the addition of the nonlinear element, can be calculated from Eq. (3a). For the modified configuration, it is valuable to calculate the natural frequency of the assembly under small displacement consideration, around $x = 0$, neglecting the nonlinearity effect, and assuming a negative stiffness of the additional element equal to k_N. The modified natural frequency can be calculated from Eq. (3b), where $f'_{n(x=0)} < f_n$ as $k_N < 0$.

$$f_n = \left(2\pi\sqrt{\frac{M}{k}}\right)^{-1}, \tag{3a}$$

$$f'_{n(x=0)} = \left(2\pi\sqrt{\frac{M}{k+k_N}}\right)^{-1}. \tag{3b}$$

The aim of this work is to utilize the natural frequency adjustment capabilities of the negative stiffness element for targeted energy transfer, from the lower parts of the building to the location of the NegSV.

3 DYNAMIC RESPONSE OF 4 STOREY BUILDING

In this section, the studied negative stiffness NegSV mechanism is fitted to a multi storey frame, as shown in Fig. 3a, with the purpose of attenuating vibrations at important components of the structure. The structure consists of 4 storeys, with a square shape plan view with dimensions 15×15 m, while all floors have 3 bays of 5 m each, in both principal directions, formed by a 4×4 square grid of columns. Respective beams and slabs are considered, while the load on all corresponding slabs is assumed to be uniformly distributed $q = 10$ kN/m^2, including self weight, permanent and live loads, resulting to a distributed mass $m_q = 1$ Mgr/m^2. The fundamental natural period period T_1 is calculated according to the proposed formula in the EC8 [22] for buildings with total height lower than 40 m:

$$T_1 = C_t \cdot H_t^{3/4}, \tag{4}$$

where H_t is the total height of the building and $C_t = 0.075$ for concrete frames. In this particular case study a concrete frame is considered with typical storey height $h_{st} = 3$ m ($H_t = 12$ m), resulting to a fundamental natural period $T_1 = 0.484$ s. The stiffness is considered identical for all storeys and is calibrated accordingly as $k_{st} = 3.15 \cdot 10^6$ kN/m, considering shear behaviour, to match the dictated first natural period. For this purpose the properties of the columns E, I are calculated as:

$$k_{cl} = \frac{12EI}{h_{st}^3} = k_{st}/N_{cl}, \tag{5}$$

where N_{cl} is the total number of columns, which in this case $N_{cl} = 16$. The modulus of elasticity is set to $E = 30$ GPa in order match the elastic properties of concrete. The moment of inertia can be calculated as $I_y = I_z = 1.5 \cdot 10^{-3}$ m^4. This is set identical in both principal directions due to symmetry. Finally, Rayleigh damping $\xi = 5\%$ is added in the building model.

The main objective of the investigation is the mitigation of inter-storey drifts towards the bottom of the structure and importantly at the first floor level, thus limiting base shear. A concept that is here explored is the tuning of the natural frequency of the top floor in a 4-storey frame to the 1st eigen-frequency of the structure. Therefore, the retrofitted storey acts as a resonator with respect to the rest of the building, where targeted energy transfer is achieved. This behaviour is followed by the disadvantage of increased drifts at the level of the modified storey. In typical buildings under base excitation, top storeys usually experience less severe loading and limited drifts. An increase of this measure at the top storey, although unfavourable, bears a less critical effect in the integrity of the building compared to the lower parts of the structure. It can also be counterbalanced by the addition of damping elements, which are responsible for dissipating energy at the location of the modification.

In the current application the mass of the top storey, which is considered as a resonator, has a significant percentage of the total mass of the structure. Therefore, simple matching of the corresponding natural frequencies does not achieve the optimal energy transfer properties. In a more accurate computation, the method proposed by Sadek et al. [23] is used for determining the stiffness and damping characteristics of the modified storey. The natural frequency and damping ratio of the additional resonator can be calculated according to Eqs. (6) and (7) respectively as:

$$f_r = \left[\frac{1}{1+\mu\Phi}\left(1 - \xi\sqrt{\frac{\mu\Phi}{1+\mu\Phi}}\right)\right] \cdot f_{n1}, \tag{6}$$

$$\zeta_r = \Phi \cdot \left(\frac{\xi}{1+\mu} + \sqrt{\frac{\mu}{1+\mu}}\right), \tag{7}$$

where f_{n1} is the first natural frequency of the primary structure, Φ is the amplitude of the first mode of vibration for participation factor equal to unity, calculated at the position of the resonator, ξ is the damping ratio of the structure and μ is calculated as:

$$\mu = \frac{m_r}{\{\phi_1\}^{\mathrm{T}}[M]\{\phi_1\}}, \tag{8}$$

where $\{\phi_1\}$ is the eigenvector of the first mode of the main structure normalized to have participation factor equal to unity and m_r is the mass of the resonator.

A resonating storey model can be effectuated by considering the main structure to include all components below the level of the added negative stiffness device, while the top storey is treated as the resonating mass. Under this approach, m_r is equal to the mass of the top storey and the stiffness of the resonator $k_r = k_{st} + k_N$. Given the original stiffness of the storey k_{st} the value of the negative stiffness k_N can be consequently calculated and the required stiffness k_d of the elements of the triangular arch can be specified depending on the geometric properties L and H. The selected properties of the arch are summarized in Table 1 and the resulting properties of the resonating storey are summarized in Table 2 respectively. The additional damping c_ν is applied to the top storey in the form of viscous dampers in order to meet the requirements of Eq. (7).

Property	Value	units
H/h_{st}	0.02	-
L	0.5	m
k_d	$1.998 \cdot 10^7$	kN/m
k_N	$-2.867 \cdot 10^5$	kN/m

Table 1: Geometric and stiffness properties of the negative stiffness device.

Property	Value	units
m_r	$225 (= m_{st})$	Mgr
k_r	$2.824 \cdot 10^4 (= k_{st} + k_N)$	kN/m
c_ν	982	Mgr/s

Table 2: Properties of the resonating storey.

3.1 Finite element model

In a first step, a finite element model is constructed, as shown in Fig. 3, using the Real-ESSI software [24]. Beams and columns are modelled with beam elements, while slabs are modelled with shell elements. Two states of the building are distinguished: state A that includes the original building, state B that includes the additional device mounted on the top storey of the building, shown in Fig. 3b. This includes the spring elements of the triangular arch (in yellow), the tip of which is connected via cables (in red) to the ceiling of the top floor. The spring elements have one end hinged to the floor of the top storey and the other end connected to a slider, able to move across one principal direction. At the equilibrium position the springs of length L_d are aligned and prestressed to length L. In equivalence to the system shown in Fig. 2, the negative stiffness results from the triangular arch, while the positive stiffness comes from

the columns on the storey. To incorporate the geometric nonlinearities that are introduced, large displacement consideration is applied to the dynamic analysis of the structure. Moreover, viscous damping elements are added connecting the tip of the arch to the nearest column, to meet the damping requirements of c_ν. Note that 4 arches operate per principal direction, while stiffness and damping requirements of the combined system should follow these of Table 1. Therefore, the stiffness of each spring element $k_d^j = 1/4 \cdot k_d$, while the viscous damping coefficient of each damper element $c_\nu^j = 1/4 \cdot c_\nu$.

Figure 3b shows the negative stiffness device in a displaced state under a horizontal static load parallel to x principal axis, applied at the level of the top slab. The nonlinear mechanisms that act parallel to the loading, along x axis, are activated and therefore, the corresponding springs are not aligned as the system is not at its initial position. To the contrary, the mechanisms acting along the y axis are not engaged under the load, being at their initial, prestressed state and therefore the corresponding springs are perfectly aligned, and the triangular arches are at their unstable equilibrium position, as shown in Fig. 3b.

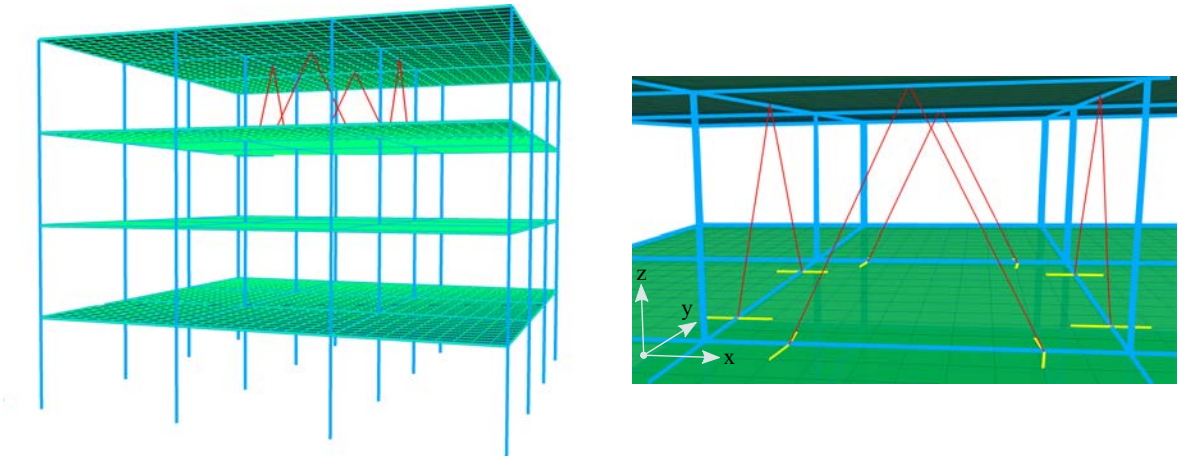

(a) Overview of the 4 storey building. (b) Displaced state of the nonlinear device.

Figure 3: Finite element model of the structure with the addition of negative stiffness device at the top (state B).

3.2 Results

The dynamic response of the system is studied under seismic input. For this purpose, base excitation is applied to the structure. In this investigation, the input is applied along one of the principal axes of the building. The input is applied to both states of the building A and B, and the results are compared.

To follow the design philosophy of codes, an artificial accelerogram is constructed, according to Ferreira et al. [25], that matches the elastic spectrum of EC8, as shown in Fig. 4. The characteristics of the target EC8 spectrum are selected as: $a_{gR} = 0.36$ g, $\gamma_{\mathrm{I}} = 1$, $S = 1.35$, and $a_g = \gamma_{\mathrm{I}} \cdot a_{gR} = 0.36$ g.

Figure 5 shows the time history results for the finite element model under base excitation according to the accelerogram of Fig. 4. Regarding the acceleration response, it is observed that it is generally mitigated in the modified building, where the negative stiffness device is in place (state B), compared to the original building (state A). This is evident in the bottom 3 floors, while the top floor experiences equivalent accelerations at both states of the frame. The inter-storey drift response shows visible reduction for the bottom 3 floors, while considerable increase of this measure is recorded for the modified, top storey. This is a result of the reduced stiffness of the

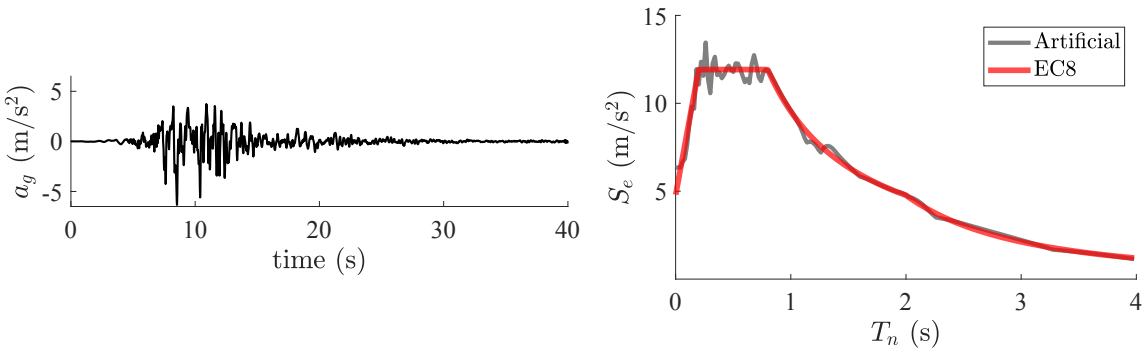

Figure 4: Artificial base excitation signal. (left)-acceleration time history, (right)-elastic response spectrum and comparison the corresponding EC8 spectrum ($a_{gR} = 0.36$ g, $\gamma_{\text{I}} = 1$, $S = 1.35$, $a_g = 0.36$ g).

storey created by the nonlinear device. However, it can be spotted that the drift ratio of that floor remains within the acceptable values of EC8 as the peak value is smaller than 1%. Critically, the drifts at the base of the structure are reduced in the modified building, a measure that is directly related to the base shear. Table 3 reports the reduction that is achieved for the acceleration and inter-storey drift measures with the use of the negative stiffness device.

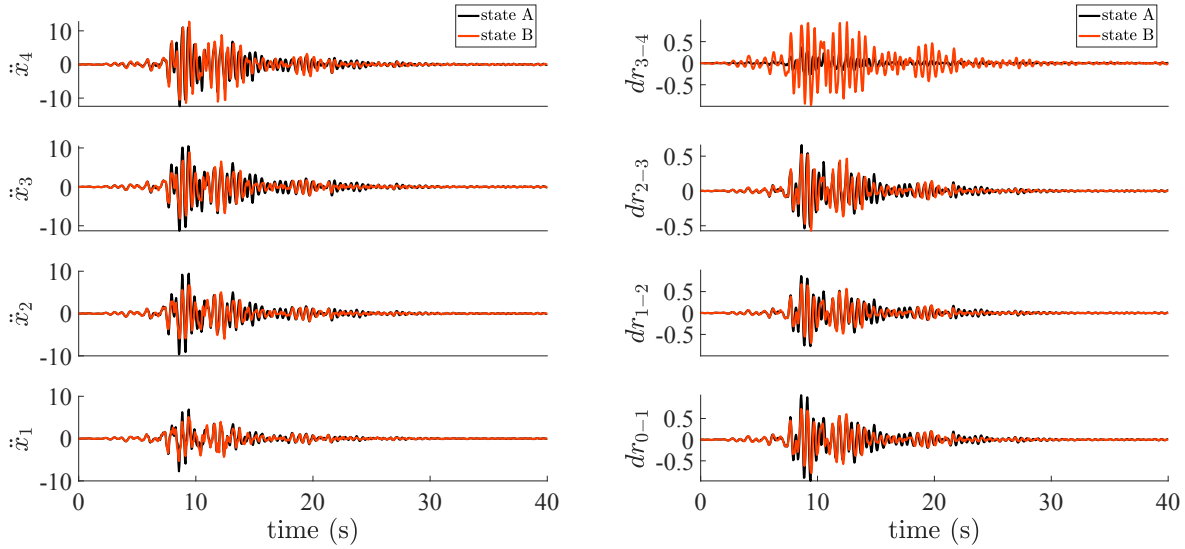

(a) Storey accelerations at level of slabs (m/s^2). (b) Inter-storey drifts ratio (%).

Figure 5: Finite element analysis results for accelerations and inter-storey drifts.

Storey No.	Acc. reduction (%)	Drift reduction (%)
1	31.4	24.9
2	30.5	19.1
3	21.6	13.1
4	-2.3	-66.2

Table 3: Reduction of the acceleration and inter-storey drift peak values for the recorded response between the original frame (state A) and the modified (state B).

4 PROBABILISTIC ASSESSMENT

In this section, the performance of the device under investigation is studied via probabilistic treatment of the seismic input. As the characteristics of each individual signal can be misleading, a generalized approach is more objective in the evaluation of the system.

4.1 Earthquake signal parametrization

Following the work of Spriridonakos et al. [26], a stochastic model is constructed for the creation of synthetic ground motions. The model involves the adoption of a white nose signal and application of a linear time-varying impulse response filter (IRF) and a time modulating filter [27]. The IRF $h[t-\tau]$ and time modulating filter $q(t,\boldsymbol{\alpha})$ take the form given in Eqs. (9) and (10) respectively.

$$h[t-\tau] = \frac{\omega_f(\tau)\mathrm{e}^{-\zeta_f\omega_f(\tau)(t-\tau)}\cdot\sin\left[\omega_f(\tau)(t-\tau)\sqrt{1-\zeta_f^2}\right]}{\sqrt{1-\zeta_f^2}}, \quad \tau\leq t \tag{9}$$

where $\omega_f(\tau)=\omega_{\text{mid}}+\omega'(\tau-t_{\text{mid}})$.

$$q(t,\boldsymbol{\alpha}) = \alpha_1 t^{\alpha_2-1}\mathrm{e}^{-\alpha_3 t}, \tag{10}$$

where $\boldsymbol{\alpha}=[\alpha_1,\alpha_2,\alpha_3]^{\mathrm{T}}$, while $\alpha_1,\alpha_3>0$, $\alpha_2>1$. The values of α_2 and α_3 can be calculated from the effective duration of the motion parameter D_{5-95} (time interval between 5% and 95% of the Arias intensity) and time t_{mid}, which is the time point, where 45% of the total Arias intensity is reached. Parameter α_1 can be consequently calculated as a function of α_2 and α_3, such that:

$$I_a = \frac{\pi}{2\mathrm{g}}\int_0^{t_n} q^2(t,\boldsymbol{\alpha})\,dt, \tag{11}$$

where I_a denotes the total Arias intensity and t_n is the total time of the ground motion.

Finally, the generated ground motion signal assumes the form:

$$x_g^p(t) = q(t,\boldsymbol{\alpha})\left\{\frac{1}{\sigma_h(t)}\int_{-\infty}^{t} h[t-\tau]w(\tau)\,d\tau\right\}, \tag{12}$$

where $w(\tau)$ is a white noise process and $\sigma_h^2(t)=\int_{-\infty}^{t}h^2[t-\tau]\,d\tau$.

Table 4 summarizes the distributions that are adopted for the individual random variables that construct the artificial signal [26, 27]. The parameters regarding the duration of the motion D_{5-95} and t_{mid} are considered deterministic, where $D_{5-95}=16.3$ s and $t_{\text{mid}}=12$ s and the total duration is $t_n=40$ s ($D_{5-95}/t_n=0.408$).

Variable	Distribution	PDF parameters
ω_{mid}	Log-logistic	$\mu=3.52,\sigma=0.24$
ω'	Logistic	$\mu=-0.052,\sigma=0.034$
ζ_f	Beta	$a=1.38,b=3.7$
$\sqrt{I_a}$	Inverse Gaussian	$\mu=0.26,\lambda=0.11$

Table 4: Random input variable distributions.

4.2 Lumped mass model

To accelerate the calculation time of the system's dynamic response, a simplified lumped mass model is created, as shown in Fig. 6a. For this purpose, concentrated masses at the slab levels are considered and the corresponding equations of motion of the system for the nonlinear case (state B) are given in Eqs. (13). The 3rd order term generated by the nonlinear mechanism appears in the connection between the two last masses. The damping coefficient c_{st} is calculated so that the system has 5% stiffness proportional damping.

$$\begin{aligned}
&m_1\ddot{x}_1 + c_{st}\left(\dot{x}_1 - \dot{x}_g\right) + k_{st}\left(x_1 - x_g\right) + c_{st}\left(\dot{x}_1 - \dot{x}_2\right) + k_{st}\left(x_1 - x_2\right) = 0\\
&m_2\ddot{x}_2 + c_{st}\left(\dot{x}_2 - \dot{x}_1\right) + k_{st}\left(x_2 - x_1\right) + c_{st}\left(\dot{x}_2 - \dot{x}_3\right) + k_{st}\left(x_2 - x_3\right) = 0\\
&m_3\ddot{x}_3 + c_{st}\left(\dot{x}_3 - \dot{x}_2\right) + k_{st}\left(x_3 - x_2\right) + \left(c_{st} + c_\nu\right)\left(\dot{x}_3 - \dot{x}_4\right) +\\
&+\left(k_{st} + k_1\right)\left(x_3 - x_4\right) + k_2(x_3 - x_4)^3 = 0\\
&m_4\ddot{x}_4 + \left(c_{st} + c_\nu\right)\left(\dot{x}_4 - \dot{x}_3\right) + \left(k_{st} + k_1\right)\left(x_4 - x_3\right) + k_2(x_4 - x_3)^3 = 0,
\end{aligned} \tag{13}$$

where $m_1 = m_2 = m_3 = m_4 = m_{st}$.

The system of Fig. 6a is simulated numerically in MATLAB® environment, with the use of $ode45$ function (AbsTol= 10^{-7}, RelTol= 10^{-7}) for the solution of the equations of motion under input base excitation x_g. A nonlinear state-space representation is subsequently constructed:

$$\begin{aligned}
&\dot{z}(t) = g(z(t), x_g(t)),\\
&z = \left[x_1, \dot{x}_1 \middle| \ldots \middle| x_4, \dot{x}_4\right]^{\mathrm{T}}.
\end{aligned} \tag{14}$$

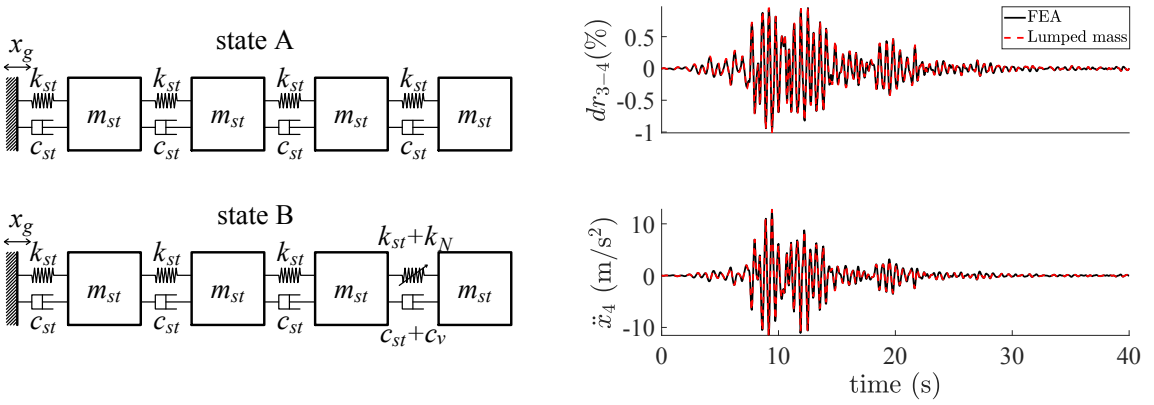

(a) Lumped mass model.

(b) Comparison of response of the state B system under base excitation between the finite element and lumped mass model solutions.

Figure 6: Lumped mass model of the 4 storey building and comparison to the results of the finite element analysis under base excitation.

Figure 6b demonstrates the comparison between the finite element and lumped mass models. The results are in agreement for the two models both in terms of displacements/drifts and accelerations. This indicates the capability of the reduced order model to capture the dynamics of the system in the linear and nonlinear state. Therefore, the simplified model is considered to offer valuable results and is used for the probabilistic assessment in this section.

4.3 Results

The performance of the system is evaluated on the mitigated response of the base of the structure and the inevitable increase of top storey drifts. To this end, a Monte Carlo analysis is performed for $N = 10^4$ simulations in order to determine the probability of exceeding the drift limits suggested by EC8 that lead to failure. For this study the inter-storey drift ratio limit is set to $dr_{\lim} = 2\%$.

Figure 7 shows the output histograms with respect to the recordings of peak inter-storey drifts for the two states of the building. For demonstration purposes, a fitted exponential distribution to each histogram is drawn in red, by calculating the maximum likelihood estimation. The main observation is the lower probability of failure in the base of the structure in the modified state that is reduced from 3.2% to 2.3%. This is achieved by the introduction of the negative stiffness device and the direction of energy away from the base. One the other hand, minor alteration on the probability of exceeding the limit value is observed for the top floor of the modified frame, compared to the original (0.5% to 0.7% respectively). Although the stiffness of the floor is reduced for state B of the structure, this is accurate for small displacement consideration. Under extensive displacements the effect of nonlinearity becomes evident, and the storey experiences a stiffening behaviour. Note in Table 1 it is selected that dimension $H = 0.02 \cdot h_{st} \Rightarrow H/h_{st} = dr_{\lim}$. Focusing on the behaviour of the nonlinear restoring force F_{tot}, shown Fig. 2b, it is observed that for displacement $x = H$ it follows that $F_{nl}(H) = 0$ and therefore $F_{tot}(H) = F_l(H)$. This effect implies that depending on the selected dimension H limitation of excessive drifts at the modified storey can be achieved, without loss of the system's functionality for small displacements. For reference, selection of $H/h_{st} = 2 \cdot dr_{\lim}$ leads to an increase of the probability of failure of the top floor to 2.7%, while reducing the probability of failure for the base to 2.0%.

Table 5 summarizes the calculated probabilities of exceeding $dr_{\lim}$ for each floor in the original and modified state A and B respectively. It is observed that considerable reduction on the probability of failure for all storeys, apart from the modified, is achieved.

Variable	state A	state B
dr_{3-4}	$\mathrm{P}_f = 0.005$	$\mathrm{P}_f = 0.007$
dr_{2-3}	$\mathrm{P}_f = 0.016$	$\mathrm{P}_f = 0.012$
dr_{1-2}	$\mathrm{P}_f = 0.025$	$\mathrm{P}_f = 0.017$
dr_{0-1}	$\mathrm{P}_f = 0.032$	$\mathrm{P}_f = 0.023$

Table 5: Probability of failure for each storey depending on drifts P_{fi} =P($dr_{i-(i-1)} > dr_{\lim}$).

5 Conclusions

In this work the vibration mitigation potential of a negative stiffness NegSV device is investigated. The system is fitted to the top floor of a 4 storey building, shifting its stiffness characteristics. The device consists of a triangular arch configuration that under large displacements yields geometric nonlinear behaviour and negative stiffness effects. Therefore, the natural frequency of the top floor can be tuned so that it matches the natural frequency of the remaining (lower level) sub-structure, essentially prompting the mass of the top floor to act as a resonator. This strategy suggests redirection of energy away from the bottom of the structure, thus reducing base shear, and dissipation at the modified floor location. This can lead to an increase in drifts at

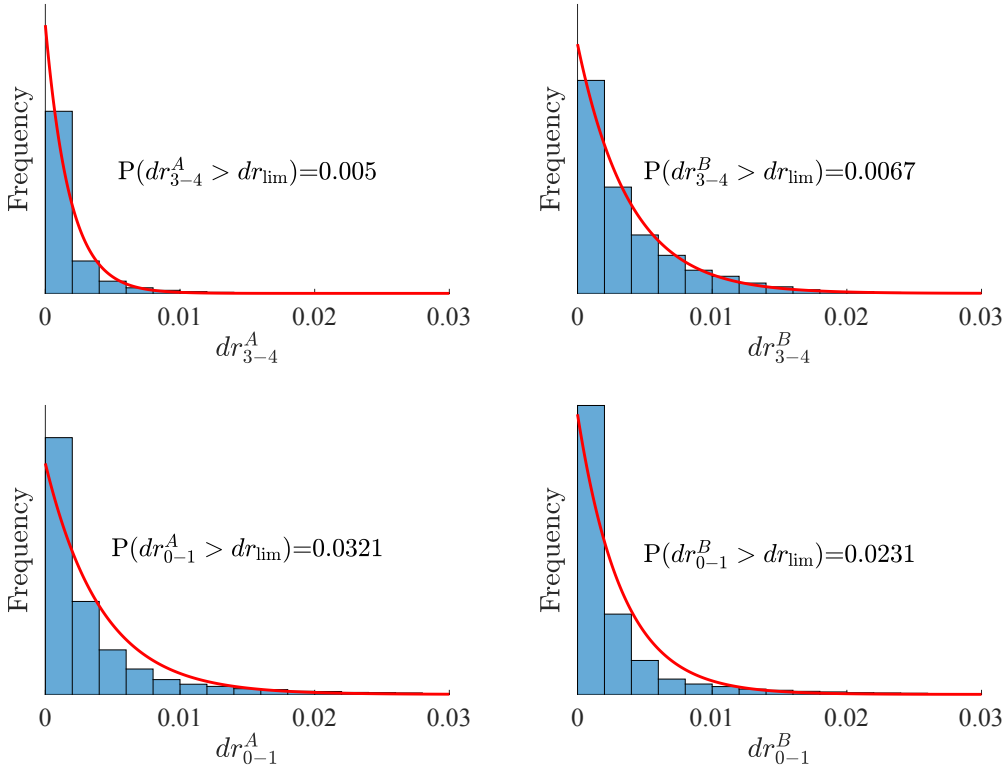

Figure 7: Histograms of the recorded maximum inter-storey drift ratios for the base dr_{0-1} and top storey dr_{3-4} and comparison between states A and B of the structure.

the modified floor, which however can be controlled to some extent by appropriate selection of the geometric properties, as demonstrated in Sec. 4.3.

The performance of the device is studied on a three dimensional frame. A detailed finite element model is created and the negative stiffness device is modelled, while the geometrically nonlinear behaviour is triggered and analysed under large displacement consideration analyses. The acceleration and inter-storey drift reduction are studied under base excitation according to an artificial accelerogram that follows the EC8 design spectrum. It is observed that both the inter-storey drifts and accelerations are mitigated in all storeys below the modification mechanism, compared to the original building. One the other hand, we observe a notable increase in the drifts, as well as a minor increase in the accelerations of the modified storey. To assess the effect of the device in a generalized manner, a probabilistic approach is applied employing parametrization of the seismic input. For this purpose, earthquake signals are treated as the output of a parametric procedure consisting of several random variables. A Monte Carlo simulation is applied for a specified sample of artificial signals. A lumped mass model is formed, which is in good agreement with the finite element model, with the purpose of accelerating the required simulation time. The probabilities for the recorded drift ratios to exceed the limit set by the provisions are calculated and compared between the original and modified building. The reduction probability of failure at the base is evidently reduced in the modified structure. It is further shown that proper selection of the geometric properties of the nonlinear mechanism

constrains the probability of exceeding the drift ratio limit at the modified storey. The current study illustrates the potential of the geometrically nonlinear NegSV device for limiting structural vibration, while comprising an actionable approach that can be applied for retrofitting of existing systems with minor intervention.

ACKNOWLEDGEMENTS

This project has received funding from the European Union's Horizon 2020 research and innovation programme under the Marie Skłodowska-Curie Grant Agreement No. 813424-INSPIRE.

REFERENCES

[1] Y. An, Z. Wang, G. Ou, S. Pan, J. Ou, Vibration Mitigation of Suspension Bridge Suspender Cables Using a Ring-Shaped Tuned Liquid Damper, Journal of Bridge Engineering 24 (4), 04019020, 2019.

[2] P. Zhang, J. Tan, H. Liu, G. Yang, C. Cui, Seismic Vibration Mitigation of a Cable-Stayed Bridge with Asymmetric Pounding Tuned Mass Damper, Mathematical Problems in Engineering 2021 (2021).

[3] M. Iqbal, A. Kumar, M. M. Jaya, O. S. Bursi, Vibration control of periodically supported pipes employing optimally designed dampers, International Journal of Mechanical Sciences 234, 107684, 2022.

[4] A. K. Chopra, Dynamics of Structures: Theory and Applications to Earthquake Engineering, Pearson, 2017.

[5] A. Y. Tuan, G. Q. Shang, Vibration control in a 101-storey building using a tuned mass damper, Journal of Applied Science and Engineering 17 (2), 141–156, 2014.

[6] V. A. Matsagar, R. S. Jangid, Base Isolation for Seismic Retrofitting of Structures, Practice Periodical on Structural Design and Construction 13 (4), 175–185, 2008.

[7] S. Nagarajaiah, K. Zou, S. Herkal, Reduction of transmissibility and increase in efficacy of vibration isolation using negative stiffness device with enhanced damping, Structural Control and Health Monitoring 29 (11), e3081, 2022.

[8] A. F. Vakakis, O. V. Gendelman, L. A. Bergman, D. M. McFarland, G. Kerschen, Y. S. Lee, Nonlinear targeted energy transfer in mechanical and structural systems I & II, Springer Netherlands, 2008.

[9] M. A. Al-Shudeifat, Highly efficient nonlinear energy sink, Nonlinear Dynamics 76 (4), 1905–1920, 2014.

[10] Y. Chen, Z. Qian, K. Chen, P. Tan, S. Tesfamariam, Seismic performance of a nonlinear energy sink with negative stiffness and sliding friction, Structural Control and Health Monitoring 26 (11), e2437, 2019.

[11] K. A. Chondrogiannis, A. Colombi, V. Dertimanis, E. Chatzi, Computational Verification and Experimental Validation of the Vibration-Attenuation Properties of a Geometrically Nonlinear Metamaterial Design, Physical Review Applied 17 (5), 054023, 2022.

[12] K. A. Chondrogiannis, V. Dertimanis, B. Jeremic, E. Chatzi, On the vibration attenuation properties of metamaterial design using negative stiffness elements, in: 2nd Internatinal Nonlinear Dynamics Conference (NODYCON 2021), Online, 2021.

[13] S. Chen, B. Wang, S. Zhu, X. Tan, J. Hu, X. Lian, L. Wang, L. Wu, A novel composite negative stiffness structure for recoverable trapping energy, Composites Part A: Applied Science and Manufacturing 129, 105697, 2020.

[14] R. Zivieri, F. Garescì, B. Azzerboni, M. Chiappini, G. Finocchio, Nonlinear dispersion relation in anharmonic periodic mass-spring and mass-in-mass systems, Journal of Sound and Vibration 462, 114929, 2019.

[15] M. Wenzel, O. S. Bursi, I. Antoniadis, Optimal finite locally resonant metafoundations enhanced with nonlinear negative stiffness elements for seismic protection of large storage tanks, Journal of Sound and Vibration 483, 115488, 2020.

[16] K. A. Chondrogiannis, V. Dertimanis, E. Chatzi, Application of Geometrically Nonlinear Metamaterial Device for Structural Vibration Mitigation, in: Conference Proceedings of the Society for Experimental Mechanics Series, Springer, 2023.

[17] K. A. Kapasakalis, I. A. Antoniadis, E. J. Sapountzakis, Performance assessment of the KDamper as a seismic Absorption Base, Structural Control and Health Monitoring 27 (4), e2482, 2020.

[18] I. A. Antoniadis, A. Paradeisiotis, Acoustic meta-materials incorporating the KDamper concept for low frequency acoustic isolation, Acta Acustica united with Acustica 104 (4), 636–646, 2018.

[19] A. G. Mantakas, K. A. Kapasakalis, A. E. Alvertos, I. A. Antoniadis, E. J. Sapountzakis, A negative stiffness dynamic base absorber for seismic retrofitting of residential buildings, Structural Control and Health Monitoring 29 (12), e3127, 2022.

[20] H. Anajafi, R. A. Medina, Partial mass isolation system for seismic vibration control of buildings, Structural Control and Health Monitoring 25 (2), e2088, 2018.

[21] M. Ziyaeifar, H. Noguchi, Partial mass isolation in tall buildings, Earthquake Engineering and Structural Dynamics 27 (1), 49–65, 1998.

[22] European Committee for Standardization, EN 1998-1: Eurocode 8: Design of structures for earthquake resistance – Part 1: General rules, seismic actions and rules for buildings (2004).

[23] F. Sadek, B. Mohraz, A. W. Taylor, R. M. Chung, A method of estimating the parameters of tuned mass dampers for seismic applications, Earthquake Engineering and Structural Dynamics 26 (6), 617–635, 1997.

[24] B. Jeremic, Z. Yang, Z. Cheng, G. Jie, N. Tafazzoli, M. Preisig, P. Tasiopoulou, F. Pisano, J. Abell, K. Watanabe, Y. Feng, S. K. Sinha, F. Behbehani, H. Yang, H. Wang, Nonlinear Finite Elements: Modelling and Simulation of Earthquakes, Soils, Structures and their Interaction, UCD and LBNL, CA, USA, 2022.

[25] F. Ferreira, C. Moutinho, Á. Cunha, E. Caetano, An artificial accelerogram generator code written in Matlab, Engineering Reports 2 (3), e12129, 2020.

[26] M. D. Spiridonakos, E. N. Chatzi, Metamodeling of nonlinear structural systems with parametric uncertainty subject to stochastic dynamic excitation, Earthquakes and Structures 8 (4), 915–934, 2015.

[27] S. Rezaeian, A. Der Kiureghian, A stochastic ground motion model with separable temporal and spectral nonstationarities, Earthquake Engineering & Structural Dynamics 37 (13), 1565–1584, 2008.